RZ 3902 (#ZUR1506-027) 06/10/2015
Physical Sciences 8 pages

Research Report

Reversible Bergman cyclization by atomic manipulation

Bruno Schuler,[1] Shadi Fatayer,[1] Fabian Mohn,[1] Nikolaj Moll,[1] Niko Pavliček,[1] Gerhard Meyer,[1] Diego Peña,[2] and Leo Gross[1]

[1]IBM Research – Zurich, 8803 Rüschlikon, Switzerland

[2]CIQUS, Universidade de Santiago de Compostela, E-15782 Santiago de Compostela, Spain

This is the author's version of the work. The definitive version was published in *Nature Chemistry*, vol. 8, no. 3, pp. 220–224 (2016) (doi: 0.1038/nchem.2438; published online 25 January 2016) and can be accessed here:
http://www.nature.com/nchem/journal/v8/n3/full/nchem.2438.html

Reversible Bergman cyclization by atomic manipulation

Bruno Schuler,[1] Shadi Fatayer,[1] Fabian Mohn,[1,*] Nikolaj Moll,[1]
Niko Pavliček,[1] Gerhard Meyer,[1] Diego Peña,[2] and Leo Gross[1,†]

[1] *IBM Research – Zurich, 8803 Rüschlikon, Switzerland*
[2] *CIQUS, Universidade de Santiago de Compostela, E-15782 Santiago de Compostela, Spain*

(Dated: August 19, 2015)

The Bergman cyclization is one of the most fascinating rearrangements in chemistry, with important implications in organic synthesis and pharmacology. Here we image a reversible Bergman cyclization for the first time. We induce the on-surface transformation of an individual aromatic diradical into a highly strained 10-membered diyne using atomic manipulation and verify the products by non-contact atomic force microscopy (AFM) with atomic resolution. The diyne and diradical were stabilized by using an ultrathin NaCl film as substrate and the diyne could be transformed back into the diradical. Importantly, diradical and diyne exhibit different reactivity, electronic, magnetic and optical properties associated to the changes in the bond topology and spin multiplicity. With the reversible, triggered Bergman cyclization we demonstrated switching on demand between the two reactive intermediates by means of selective C–C bond formation or cleavage, opening up the entire field of radical chemistry for on-surface reactions by atomic manipulation.

In a pioneering work from 1972[1], Jones and Bergman explained the thermal isomerization of deuterated enediynes **1** and **3** by proposing a rearrangement reaction through diradical **2** (1,4-didehydrobenzene or *para*-benzyne), the so-called Bergman cyclization[2] (see Fig. 1a). The importance of this reaction was recognized when enediyne anticancer antibiotics were discovered in the late 1980s[3,4]. In particular, these molecules are thought to cleave the double-stranded DNA by a mechanism of action based on the generation and subsequent reaction of 1,4-diradicals[5]. Remarkably, the enediyne moiety in these anticancer drugs is embedded in a 9- or 10-membered ring, which favors the cyclization reaction. In this respect, Bergman cyclizations of strained cyclic diynes have been widely studied. For example, Masamune *et al.* attempted to synthesize highly reactive diyne **4** in solution, resulting in the isolation of anthracene[6]. Afterwards, several groups described the spectroscopic characterization of transient diyne **4**[7–9], while Sander *et al.* reported its matrix isolation[10].

In recent years, on-surface synthesis has been successfully applied to prepare diverse nanostructures following bottom-up approaches[11,12]. Among the reactions employed for this purpose, the Ullmann coupling of halogenated aromatic compounds has emerged as the most successful on-surface chemical transformation[13–16]. In most cases, this reaction is thought to proceed via dehalogenation of aryl halides followed by C–C coupling of the resulting aryl radicals. Moreover, Bergman cyclizations have also been proposed to play a role in the on-surface synthesis of polyphenylene chains[17] and cyclization of oligo-(phenylene-1,2-ethynylenes)[18].

Scanning tunnelling microscopy (STM) made it possible to trigger and image reactions at the level of individual molecules[13,19–25]. The direct visualization of the chemical structure with AFM using functionalized tips[26] was used to observe bond making and breaking in a metal–molecule complex[27], to investigate the molecular structure of reactive intermediates formed by atomic manipulation[28], and to identify products formed by on-surface chemistry[18,29].

In this study, a highly strained 10-membered ring diyne **4** was generated by a sequence of single-molecule reactions involving two reaction intermediates from 9,10-dibromoanthracene (DBA **6**) on a bilayer NaCl film on Cu(111). First, DBA was selectively debrominated one-by-one to form a didehydroanthracene diradical **5**, subsequently a ring-opening retro-Bergman cyclization was initiated, all by means of atomic manipulation. The structures of the reaction product and intermediates were identified and characterized using AFM. We demonstrate the reversible conversion between diradical and diyne, realizing a tri-state single molecular switch based on forward and backward Bergman reaction[1,2] (see Fig. 1b).

Results and Discussion

We deposited DBA on a Cu(111) surface, partly covered by NaCl islands of mainly two monolayer thickness, denoted as NaCl(2ML)/Cu(111). Deposition of molecules with submonolayer coverage at a sample temperature of approximately 10 K led to individual DBA molecules adsorbed on the surface. We used AFM imaging with CO tips[26] to resolve the chemical structure of the precursor (Fig. 2a), and identify intermediates (Figs. 2b,c) and the reaction product (Fig. 2d).

As seen in Fig. 2e the Br atoms of DBA appear as bright lobes of increased frequency shift. We dissociated the Br atoms on NaCl(2ML)/Cu(111) by placing the

tip above the molecule and applying a voltage pulse. The voltage threshold to dissociate the first Br atom, which forms 9-dehydro-10-bromoanthracene (radical **7**) is about 1.6 V. In the AFM image of the bromoanthryl radical, shown in Fig. 2f, the bright feature corresponding to the Br atom can only be seen on one side of the molecule. The contrast of the molecule indicates that its adsorption is non-planar with a reduced adsorption height of the debrominated side of the molecule[30,31].

The second C–Br bond was cleaved to form the non-Kekulé hydrocarbon diradical **5** by applying a voltage pulse of about 3.3 V; thereby the tip was retracted by several Ångströms to limit the current to tens of picoamperes. The dissociation processes of both Br were often accompanied by displacements of the organic fragment and the Br atoms[32]. The AFM image of the diradical is shown in Fig. 2g. As demonstrated for *ortho*-arynes, the NaCl film facilitates the stabilization of reactive intermediates such as radicals and diradicals[28]. Next, a voltage pulse of 1.7 V was applied with the tip above the diradical. AFM imaging of the resulting product, shown in Fig. 2h, revealed a molecule apparently consisting of a fused 6- and a 10-membered ring, suggesting the formation of diyne **4** by homolytic cleavage of the C–C bond shared by two fused benzene rings. Note that this diyne was often created directly from the radical without first observing diradical **5**.

To prove that we indeed created the cyclic diyne, we employed a combination of STM for orbital imaging[33] (Fig. 3a), CO tip AFM images at different tip heights (Figs. 3b-d) and compared the experiments with density functional theory (DFT) calculations (Figs. 3e-h). With orbital imaging, only the negative ion resonance, corresponding to the lowest unoccupied molecular orbital (LUMO), was in the experimentally accessible voltage range without switching or displacing the molecule. The relative orbital intensities and the location of the nodal planes are in good agreement with the calculated LUMO of diyne (Fig. 3e), corroborating our assignment.

The experimental and calculated AFM images of the 10-membered carbon ring of the diyne exhibits features that relate to different bond orders[34] and that lead to a characteristic fingerprint of this moiety. For example the triple bonds of the structure in Fig. 2d appear with a distinctive elongation perpendicular to the bond direction as previously found for alkynes imaged by CO tips[18,35]. In the Supplementary Information a detailed bond-order analysis of diyne and the diradical is provided. Also, the benzene ring appears more pronounced in both the measurement and calculation as a result of a small upwards bending of the ring. On the metal the diradical could be generated but no diyne creation was observed, emphasizing the importance of the insulating layer to stabilize the reactive intermediates[28] and to facilitate the reaction. Instead, the diradical binds to the substrate at the center of the molecule on Cu(111) (see Fig. S1). The direct visualization of the molecular structures by AFM and the good agreement of theoretical calculations with AFM and STM images prove the creation of diyne and thus the successful execution of a retro-Bergman cyclization using atomic manipulation.

Next, we study the Bergman cyclization reaction in more detail and demonstrate its reversibility and the inter-conversion between the two possible diyne topomers: diyne **4R**, with the 10-membered ring on the right hand side, and diyne **4L**, with this ring on the left (see Fig. 4). Which topomer is created depends on which of the two C–C bonds that are shared by fused benzene rings is cleaved. To avoid displacements of the molecule accompanied with switching, we stabilized the diradical at a step edge of a third-layer NaCl island. To this end, we first manipulated the molecule by inelastic excitation[36] to bring the molecule to a NaCl step edge shown in Fig. 4. The bright features seen in the bottom part of Figs. 4a-c correspond to the Cl ions in the third NaCl layer[37]. In the current trace recorded during such switching at 1.64 V (Fig. 4d) we observe switching between three distinct current levels. By reducing the voltage after switching of the molecule and taking an AFM image, we can relate the three different current plateaus in Fig. 4d to the molecular structures shown in Figs. 4a-c. Fig. 4a shows diyne **4R** and corresponds to the low-current state in Fig. 4d. Fig. 4b shows the diradical corresponding to the medium-current state and Fig. 4c shows diyne **4L**, which corresponds to the high-current state in Fig. 4d. Note that the lateral tip position determines the value of the current plateaus measured above the different isomers. As indicated by the white circle in Fig. 4b we chose an off-centered position in order to distinguish diyne **4L** from diyne **4R**. The voltage threshold for the Bergman cyclization to take place is close to the LUMO orbital energy of the diyne molecule, which suggests that the process is initiated by an electron attachment. The switching yield per electron depends on the environment, in particular on the adsorption at the step edge breaking the symmetry of the molecule. Note that the switching trace in Fig. 4d indicates that there is no direct transition between the two different diyne topomers. But the topomer interconversion involves always the diradical as an intermediate.

These observations demonstrate that the Bergman reaction can be performed reversibly in this system, that is, the two C–C bonds shared by two fused benzene rings within the molecule can be created and cleaved again. Note that we cannot direct in which state the molecule will switch, but we can stop the switching in any of

the three molecular states at will. When reducing the voltage below the reaction threshold all three molecular structures remain stable and no switching was observed enabling the recording of AFM images at low voltage.

We calculated the potential energy surface of the Bergman cyclization of the free molecule (Fig. 4e gray and black curve) and the molecule adsorbed on NaCl/Cu(111) (Fig. 4e orange and red curve) by DFT, using the carbon–carbon distance of the bond that is formed during the Bergman reaction as the reaction coordinate. Particularly, the effect of spin multiplicity (singlet or triplet) is studied by spin-polarized energy minimization. For both the free molecule and the molecule adsorbed on the surface, the diradical and the diyne form two (meta)stable states. In vacuum, diyne has a lower absolute energy compared to the diradical by 0.51 eV, with a barrier of 0.67 eV, which is similar to the values reported previously[10]. Interestingly, in the diradical structure the triplet state is slightly preferred over the singlet. On the surface, the diradical energy is significantly lowered for both singlet and triplet state. Consequently, the diradical triplet and the diyne singlet have now approximately the same energy. Additionally, the singlet–triplet splitting of the diradical, 0.15 eV on the surface, is increased compared to vacuum. The comparable energy of diradical and diyne on the surface and the substantial energy barrier separating the two states allows us to stabilize both states individually in experiment.

Conclusions

We demonstrated the sequential on-surface synthesis of a strained diyne by three consecutive single-molecule reactions starting from DBA by means of atomic manipulation. The reaction intermediates and product were unambiguously identified and were characterized by atomic resolution AFM measurements, STM orbital imaging and DFT calculations. The diradical–diyne conversion represents a retro-Bergman cyclization that can be triggered reversibly and involves two diyne topomers, constituting a tri-state molecular switch. Interestingly, the *para*-coupled aromatic diradical has a triplet ground state, which makes this system of potential use as a switchable single-molecule magnet controlled by its molecular structure.

METHODS

Experimental details

Setup The experiments were performed using a home-built low-temperature ($T \approx 5\,\mathrm{K}$), ultra-high vacuum ($p \approx 10^{-10}\,\mathrm{mbar}$) combined STM and AFM. The sensor was based on a qPlus[38] quartz-crystal cantilever design operated in the frequency-modulation mode[39] (resonance frequency $f_0 \approx 30\,\mathrm{kHz}$, spring constant $k \approx 1800\,\mathrm{N/m}$, quality factor $Q \approx 14,000$, and oscillation amplitude $A \approx 0.5\,\mathrm{Å}$). The voltage was applied to the sample. STM images were taken in constant-current mode. AFM measurements were acquired in constant-height mode at $V = 0\,\mathrm{V}$. The experimental tip height was related to the tip–molecule distance by setting the tip height at the $\Delta f(z)$ minimum above the benzene ring to $z = 3.9\,\mathrm{Å}$[34].

Sample preparation First, a Cu(111) single crystal was cleaned by repeated sputtering (Ne^+) and annealing (900 K) cycles. Subsequently, NaCl was evaporated at about 270 K, such that (100)-oriented NaCl islands of mostly two atomic layers in thickness were formed. A low coverage (approximately $0.01\,\mathrm{nm}^{-2}$) of CO was deposited on the surface (at $T \approx 10\,\mathrm{K}$) for tip preparation by admitting CO into the UHV chamber. The DBA molecules were sublimed by flash-heating the solid compound from a piece of Si wafer onto the sample (at $T \approx 10\,\mathrm{K}$).

Tip preparation For the microscope tip we used a 25 μm-thick PtIr wire, sharpened with a focused ion beam. Thereafter, we prepared a clean and sharp Cu tip by repeated indentations into the Cu surface. A CO tip was created by picking-up a single CO molecule from the surface[26,32]. Apparent distortions of the molecular structure in AFM images result from the CO tilting at the tip[34,40,41].

Density-functional theory (DFT) calculations

The adsorption geometry of the diradical and diyne molecules on a bilayer NaCl film on Cu(100) were calculated with DFT[42]. The Cu(100) surface was used for the calculations because NaCl is commensurate for this surface orientation, leading to smaller super cells. A code with numerical atomic orbitals as basis functions[43] and the Perdew-Burke-Ernzerhof exchange-correlation functional (PBE)[44] was applied. A van der Waals method[45] combined with the Lifshitz-Zaremba-Kohn theory for the nonlocal Coulomb screening within the bulk for the Cu substrate[46] and calculated coefficients for *atoms in the solid*[47] for the NaCl film were used. The energy of the triplet state is calculated by performing spin-polarized energy minimization where the spin of the entire unit cell is constrained to a spin multiplicity of three. The slab to model the NaCl surface consisted of four layers of Cu substrate with a (001) surface with two layers of NaCl film on top. The (x,y,z) dimension of the calculated cell was (23.10 Å, 15.40 Å, 29.04 Å). The NaCl layers and the two topmost Cu layers were fully relaxed.

We found that in the calculations both the diradical and diyne molecules adsorb with their long axis along a row of Cl atoms in the [011] direction (in agreement with the experiments). For the diradical the two outer benzene rings are bent downwards, so that the outermost C atoms are 0.1 Å closer to the substrate than the inner ones. The diyne 10-membered ring bent downwards, so that the outermost C atoms are 0.14 Å closer to the substrate than the 6-membered ring.

We calculated the Bergman cyclization energies by taking the C–C bond length $d_{C\text{-}C}$ as the reaction coordinate and fixing it to different values.

The frequency shift spectra were calculated without the underlying substrate but keeping the atomic positions of the two molecules fixed as found in the adsorption geometry calculated on the substrate. Otherwise, the computational time would be prohibitively long. We calculated the total energy of the molecules interacting with a vertical Cu-dimer tip functionalized with a CO[34]. We used the Cu-dimer as the metallic part of the tip in our calculations, because it shows spherical symmetry, and the small number of atoms reduces the computational costs. By changing the length of the Cu dimer the spring constant can be tuned between 0.9 N/m and 0 N/m. Here, we used a dimer length of 2.75 Å which leads to a very small intrinsic spring constant of 0.03 N/m. The vertical attractive forces will, however, lead to an additional position dependent spring constant of up to 0.26 N/m. To obtain the frequency shift we took the second derivative with respect to the z-direction.

* Permanent address: ABB Corporate Research, 5405 Baden-Dättwil, Switzerland.
† lgr@zurich.ibm.com

[1] Jones, R. R. & Bergman, R. G. p-Benzyne. Generation as an intermediate in a thermal isomerization reaction and trapping evidence for the 1,4-benzenediyl structure. *J. Am. Chem. Soc.* **94**, 660–661 (1972).
[2] Wenk, H. H., Winkler, M. & Sander, W. One century of aryne chemistry. *Angew. Chem., Int. Ed.* **42**, 502–528 (2003).
[3] Nicolaou, K. C., Dai, W.-M., Tsay, S.-C., Estevez, V. A. & Wrasidlo, W. Designed enediynes: A new class of dna-cleaving molecules with potent and selective anticancer activity. *Science* **256**, 1172–1178 (1992).
[4] Nicolaou, K., Smith, A. & Yue, E. Chemistry and biology of natural and designed enediynes. *Proc. Natl. Acad. Sci.* **90**, 5881–5888 (1993).
[5] Sinha, S. C. *et al.* Prodrugs of dynemicin analogs for selective chemotherapy mediated by an aldolase catalytic ab. *Proc. Natl. Acad. Sci. USA* **101**, 3095–3099 (2004).
[6] Darby, N. *et al.* Concerning the 1,5-didehydro [10] annulene system. *J. Chem. Soc. (D)* **23**, 1516–1517 (1971).
[7] Chapman, O., Chang, C. & Kolc, J. 9,10-Dehydroanthracene. A derivative of 1,4-dehydrobenzene. *J. Am. Chem. Soc.* **98**, 5703–5705 (1976).
[8] Schottelius, M. J. & Chen, P. 9,10-dehydroanthracene: p-benzyne-type biradicals abstract hydrogen unusually slowly. *J. Am. Chem. Soc.* **118**, 4896–4903 (1996).
[9] Wenk, H. H. & Sander, W. Photochemistry of 9,10-dicarbonyl-9,10-dihydroanthracene a source of 9,10-dehydroanthracene? *Eur. J. Org. Chem.* **1999**, 57–60 (1999).
[10] Kötting, C., Sander, W., Kammermeier, S. & Herges, R. Matrix isolation of 3,4-benzocyclodeca-3,7,9-triene-1,5-diyne. *Eur. J. Org. Chem.* **1998**, 799–803 (1998).
[11] Perepichka, D. F. & Rosei, F. Extending polymer conjugation into the second dimension. *Science* **323**, 216–217 (2009).
[12] Palma, C.-A. & Samorì, P. Blueprinting macromolecular electronics. *Nat. Chem.* **3**, 431–436 (2011).
[13] Hla, S.-W., Bartels, L., Meyer, G. & Rieder, K.-H. Inducing all steps of a chemical reaction with the scanning tunneling microscope tip: Towards single molecule engineering. *Phys. Rev. Lett.* **85**, 2777 (2000).
[14] Grill, L. *et al.* Nano-architectures by covalent assembly of molecular building blocks. *Nat. Nanotechnol.* **2**, 687–691 (2007).
[15] Cai, J. *et al.* Atomically precise bottom-up fabrication of graphene nanoribbons. *Nature* **466**, 470–473 (2010).
[16] Lafferentz, L. *et al.* Controlling on-surface polymerization by hierarchical and substrate-directed growth. *Nature Chem.* **4**, 215–220 (2012).
[17] Sun, Q. *et al.* On-surface formation of one-dimensional polyphenylene through Bergman cyclization. *J. Am. Chem. Soc.* **135**, 8448–8451 (2013).
[18] de Oteyza, D. G. *et al.* Direct imaging of covalent bond structure in single-molecule chemical reactions. *Science* **340**, 1434–1437 (2013).
[19] Stipe, B. *et al.* Single-molecule dissociation by tunneling electrons. *Phys. Rev. Lett.* **78**, 4410 (1997).
[20] Lee, H. J. & Ho, W. Single-bond formation and characterization with a scanning tunneling microscope. *Science* **286**, 1719–1722 (1999).
[21] Zhao, A. *et al.* Controlling the Kondo effect of an adsorbed magnetic ion through its chemical bonding. *Science* **309**, 1542–1544 (2005).
[22] Repp, J., Meyer, G., Paavilainen, S., Olsson, F. E. & Persson, M. Imaging bond formation between a gold atom and pentacene on an insulating surface. *Science* **312**, 1196 (2006).
[23] Liljeroth, P., Repp, J. & Meyer, G. Current-induced hydrogen tautomerization and conductance switching of naphthalocyanine molecules. *Science* **317**, 1203 (2007).
[24] Albrecht, F., Neu, M., Quest, C., Swart, I. & Repp, J. Formation and characterization of a molecule–metal–molecule bridge in real space. *J. Am. Chem. Soc.* **135**, 9200–9203 (2013).
[25] Kumagai, T. *et al.* Controlling intramolecular hydrogen transfer in a porphycene molecule with single atoms or molecules located nearby. *Nature Chem.* **6**, 41–46 (2014).
[26] Gross, L., Mohn, F., Moll, N., Liljeroth, P. & Meyer, G. The chemical structure of a molecule resolved by atomic force microscopy. *Science* **325**, 1110 (2009).
[27] Mohn, F. *et al.* Reversible bond formation in a gold-atom–organic-molecule complex as a molecular switch. *Phys. Rev. Lett.* **105**, 266102 (2010).
[28] Pavlicek, N. *et al.* On-surface generation and imaging of arynes by atomic force microscopy. *Nature Chem.* **7**, 623–628 (2015).
[29] Riss, A. *et al.* Local electronic and chemical structure of oligo-acetylene derivatives formed through radical cyclizations at a surface. *Nano Lett.* **14**, 2251–2255 (2014).
[30] Pavliček, N. *et al.* Atomic force microscopy reveals bistable configurations of dibenzo[a,h]thianthrene and their interconversion pathway. *Phys. Rev. Lett.* **108**, 086101 (2012).
[31] Schuler, B. *et al.* Adsorption geometry determination of single molecules by atomic force microscopy. *Phys. Rev. Lett.* **111**, 106103 (2013).
[32] Mohn, F., Schuler, B., Gross, L. & Meyer, G. Different

tips for high-resolution AFM and STM imaging of single molecules. *Appl. Phys. Lett.* **102**, 073109 (2013).
[33] Repp, G., Meyer, G., Stojkovic, S. M., Gourdon, A. & Joachim, C. Molecules on insulating films: Scanning-tunneling microscopy imaging of individual molecular orbitals. *Phys. Rev. Lett.* **94**, 026803 (2005).
[34] Gross, L. *et al.* Bond-order discrimination by atomic force microscopy. *Science* **337**, 1326 (2012).
[35] Moll, N. *et al.* Image distortions of partly fluorinated hydrocarbons in atomic force microscopy with carbon monoxide terminated tips. *Nano Lett.* **14**, 61276131 (2014).
[36] Swart, I., Sonnleitner, T., Niedenführ, J. & Repp, J. Controlled lateral manipulation of molecules on insulating films by STM. *Nano Lett.* **12**, 1070–1074 (2012).
[37] Gross, L. *et al.* Organic structure determination using atomic resolution scanning probe microscopy. *Nature Chem.* **2**, 821 (2010).
[38] Giessibl, F. J. High-speed force sensor for force microscopy and profilometry utilizing a quartz tuning fork. *Appl. Phys. Lett.* **73**, 3956 (1998).
[39] Albrecht, T. R., Grütter, P., Horne, D. & Rugar, D. Frequency modulation detection using high-Q cantilevers for enhanced force microscope sensitivity. *J. Appl. Phys.* **69**, 668–673 (1991).
[40] Boneschanscher, M. P., Hämäläinen, S. K., Liljeroth, P. & Swart, I. Sample corrugation affects the apparent bond lengths in atomic force microscopy. *ACS Nano* **8**, 3006–3014 (2014).
[41] Hapala, P. *et al.* The mechanism of high-resolution STM/AFM imaging with functionalized tips. *Phys. Rev. B* **90**, 085421 (2014).
[42] Hohenberg, P. & Kohn, W. Inhomogeneous electron gas. *Phys. Rev.* **136**, B864–B871 (1964).
[43] Blum, V. *et al.* Ab initio molecular simulations with numeric atom-centered orbitals. *Comp. Phys. Comm.* **180**, 2175–2196 (2009).
[44] Perdew, J. P., Burke, K. & Ernzerhof, M. Generalized gradient approximation made simple. *Phys. Rev. Lett.* **77**, 3865–3868 (1996).
[45] Tkatchenko, A. & Scheffler, M. Accurate molecular van der Waals interactions from ground-state electron density and free-atom reference data. *Phys. Rev. Lett.* **102**, 073005 (2009).
[46] Ruiz, V. G., Liu, W., Zojer, E., Scheffler, M. & Tkatchenko, A. Density-functional theory with screened van-der-Waals interactions for the modeling of hybrid inorganic-organic systems. *Phys. Rev. Lett.* **108**, 146103 (2012).
[47] Zhang, G.-X., Tkatchenko, A., Paier, J., Appel, H. & Scheffler, M. Van der Waals interactions in ionic and semiconductor solids. *Phys. Rev. Lett.* **107**, 245501 (2011).

ACKNOWLEDGMENTS

We thank Ivano Tavernelli, Dolores Pérez, Enrique Guitán and Rolf Allenspach for discussions. We acknowledge financial support from the ERC Advanced Grant CEMAS (agreement no. 291194), EU project PAMS (610446) and ITNs qTea (317485) and ACRITAS (317348). D.P. acknowledges the Spanish Ministry of Science and Competitiveness for financial support (MAT2013-46593-C6-6-P).

AUTHOR CONTRIBUTIONS

B. S., S. F., F. M., N. P., G. M. and L. G. performed the STM/AFM experiments. N. M. performed the DFT calculations. All authors analyzed the data and contributed to the manuscript.

ADDITIONAL INFORMATION

Supplementary information is available in the online version of the paper. Reprints and permissions information is available online at www.nature.com/reprints. Correspondence and requests for materials should be addressed to L.G.

COMPETING FINANCIAL INTERESTS

The authors declare no competing financial interests.

FIGURES

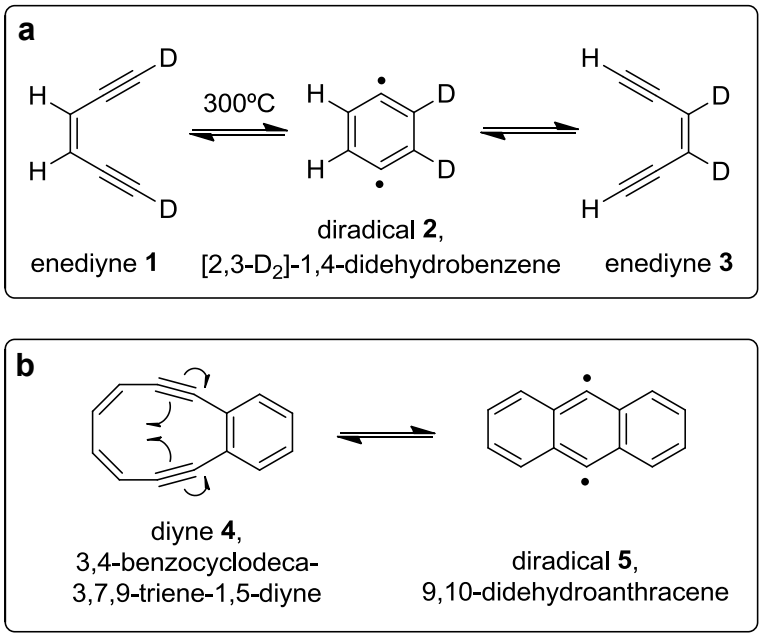

FIG. 1. **Bergman cyclizations. a** Seminal experiment regarding the thermal isomerization of deuterated enediynes **1** and **3** through the formation of diradical **2**[1]. **b** Bergman cyclization of cyclic diyne **4** to generate diradical **5**.

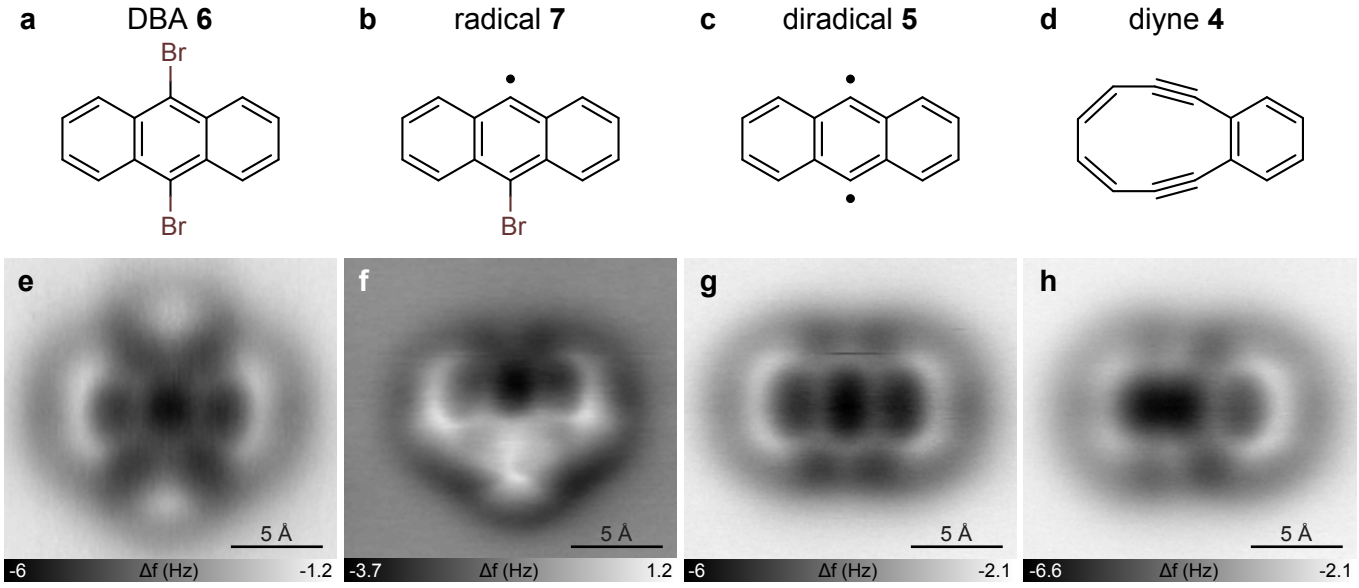

FIG. 2. **Structures and AFM imaging of the starting material, reaction intermediates and product. a-d** Chemical structures of the reaction products formed by successive STM-induced debromination of 9,10-dibromoanthracene (DBA) and subsequent retro-Bergman cyclization: DBA, 9-dehydro-10-bromoanthracene (radical), 9,10-didehydroanthracene (diradical) and 3,4-benzocyclodeca-3,7,9-triene-1,5-diyne (diyne). **e-h** Corresponding constant-height AFM images of the molecules in **a-d** on NaCl(2ML)/Cu(111) using a CO tip.

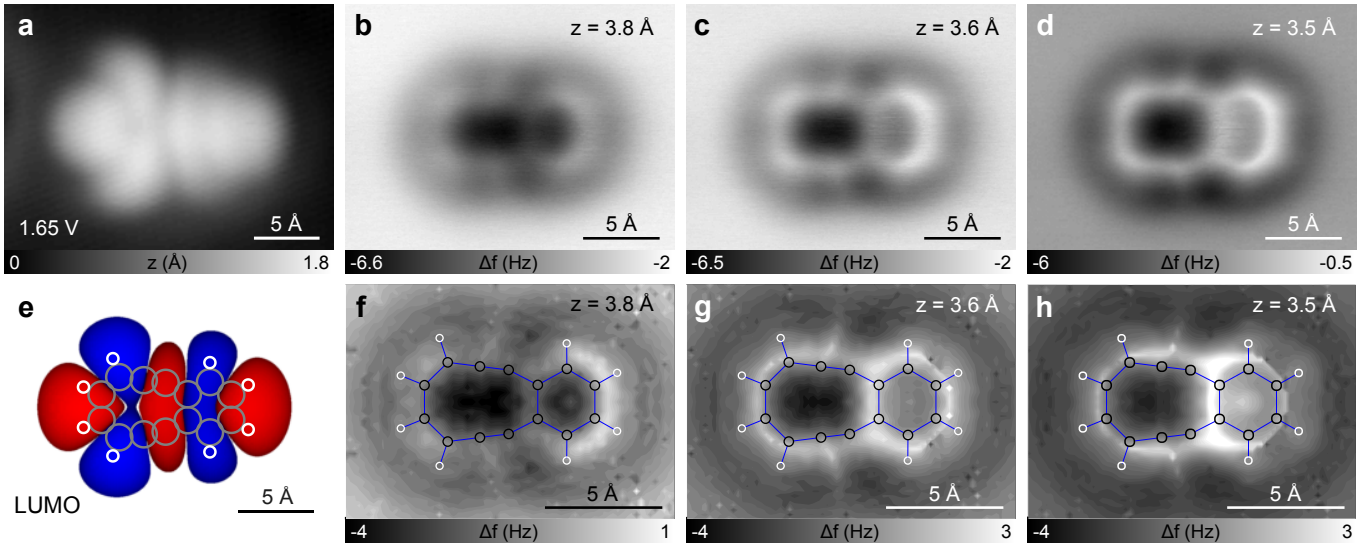

FIG. 3. **Diyne identification.** **a** Constant-current STM image ($I = 2\,\mathrm{pA}$, $V = 1.65\,\mathrm{V}$) of diyne. **b-d** Constant-height AFM images of diyne on NaCl(2ML)/Cu(111) at different heights z. **e** Calculated LUMO orbital of diyne with the molecular structure overlaid as a guide to the eye. **f-h** Calculated Δf maps of diyne interacting with a CO tip, at tip–molecule distances corresponding to estimated experimental distances in **b-d**.

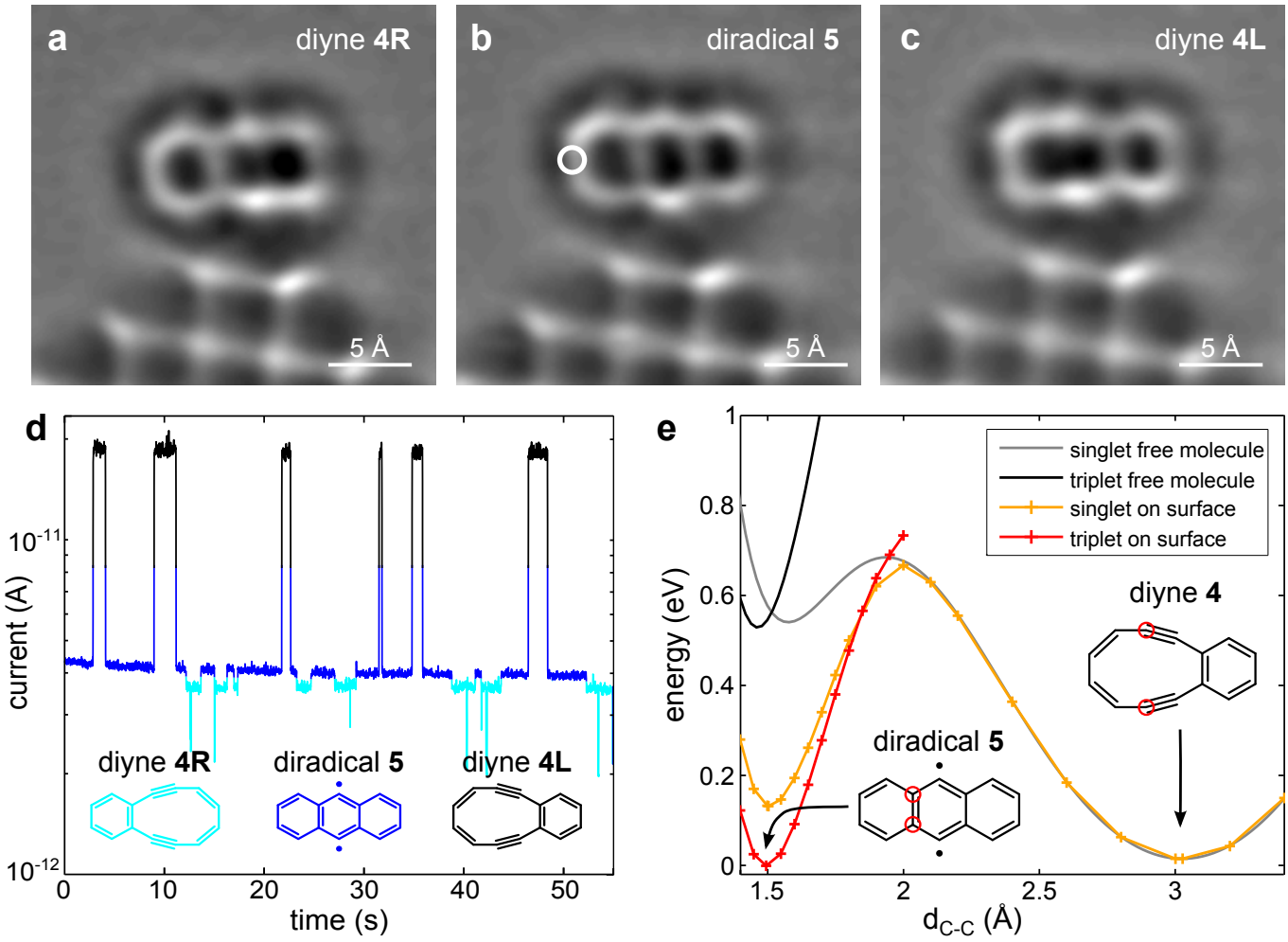

FIG. 4. **Reversible Bergman cyclization. a-c** Laplace-filtered AFM images of diyne **4R** (**a**), diradical **5** (**b**) and diyne **4L** (**c**) on NaCl(2ML)/Cu(111). The molecule is adsorbed at a step edge of an NaCl(3ML)/Cu(111) island, seen in the lower part of the image. **d** Current trace during a voltage pulse of $V = 1.64\,\mathrm{V}$ at the position indicated by the white circle in **b**. The different current levels correspond to the molecular structures of the same color shown in the inset. **e** Calculated energies of the Bergman cyclization, using the carbon–carbon distance $d_{\mathrm{C\text{-}C}}$ of the carbons indicated by the red circles as a reaction coordinate.